Article

Open Access

MULTISCIA
JOURNALS PUBLISHERS

FRONTIERS IN PHARMACEUTICAL ANALYSIS

ISSN: (3065- 1352)

https://multisciajournals.com/journals/index.php/fpa

editor.fpa1@gmail.com

Frontiers in Zoological Research
Volume 1 Issue 2 2025

Through the mir-130b-5p/ASH1L pathway, CircSHOC2 controls the production of steroid hormones in ovarian granulosa cells.

P Sujatha, P Dhavachelvan
Department of **Zoological Research**

Article Info

Received: 30-4-2025 Revised:08-06-2025 Accepted:19-06-2025 Published:29-06-2025

ABSTRACT

A crucial stage of the pig reproductive cycle, estrus depends on coordinated steroidogenesis and healthy ovarian growth. By secreting progesterone (P4) and estradiol (E2), which are necessary for follicular maturation and ovulatory competence, granulosa cells (GCs) mediate these processes. Circular RNAs (circRNAs) have been linked to the manufacture of steroid hormones, although it is yet unknown how they affect the estrous control. Circular SHOC2 leucine rich repeat scaffold protein (circSHOC2) is a novel circRNA that was identified in this study by performing circRNA sequencing on ovarian tissues of estrous (ES) and non-estrous (NES) gilts. The circRNA was found to be significantly up-regulated in ES ovaries. Functional tests showed that overexpression of circSHOC2 boosted the protein levels of important steroidogenic enzymes and improved the synthesis of E2 and P4. According to mechanistic analysis, circSHOC2 sponges miR-130b-5p. Steroidogenic proteins were up-regulated and E2 and P4 synthesis were markedly increased when miR-130b-5p was silenced. Furthermore, ASH1-like histone lysine methyltransferase (ASH1L) was the target of miR-130b-5p, and ASH1L was markedly suppressed by its overexpression. ASH1L reduced the inhibitory effects of miR-130b-5p on E2 and P4 production in GCs, according to cotransfection investigations. These results provide mechanistic insight into the molecular basis of gilt estrus and provide targets to improve reproductive efficiency by establishing a regulatory axis in which circSHOC2 controls steroidogenic capacity in pig GCs via the miR-130b-5p/ASH1L pathway. Keywords: CircRNA, miR-130b-5p, ASH1L, steroid hormone, and gilt estrus,

Introduction:

The profitability of commercial swine production is strongly impacted by efficient gilt reproduction, which is the foundation of herd productivity. Nevertheless, 10% of gilts are removed from breeding programs after failing to show their first estrus by the age of 8 months (Xin et al., 2018). Follicle growth in the ovary controls the commencement of estrous, when estrogen produced by granulosa cells (GC) instructs the brain to start estrous activity (Dial et al., 1983). One of the main reasons gilts experience estrous failure is impaired follicular development, which interferes with steroidogenesis (Knox, 2024; Langendijk et al., 2000). The primary steroid hormones produced by ovarian GCs are progesterone (P4) and estradiol (E2) (Feng et al., 2019; Kolesarova et al., 2017; Rodway et al., 1999; Sirotkin, 1994). These hormones are crucial for promoting early pregnancy (Geisert et al., 2024), controlling estrous cyclicity (Domingues et al., 2023), and coordinating follicular maturation (Ting et al., 2015). The exact mechanisms behind regulatory networks are still unclear, despite the fact that environmental influences (Knox, 2024), dietary state (Xiong et al., 2024), and genetic predisposition (Liu et al., 2024) all have an impact

on steroid hormone synthesis. Therefore, increasing steroidogenic production in GCs presents a viable approach to encourage the start of estrus and boost gilt reproductive efficiency (Am-In et al., 2020; Ziecik et al., 2020). The expression patterns of circular RNAs (circRNAs), a subclass of noncoding RNAs (ncRNAs), are known to be tissue-, cell-, and developmental stage-specific (Jeck et al., 2013; Ma et al., 2023). Across a range of species, including mice (Jia et al., 2018), pigs (Liang et al., 2017), cattle (Fu et al., 2018), and goats (Xu et al., 2021), numerous investigations have reported circRNA expression variations throughout ovarian development, folliculogenesis, and the estrous cycle. Although these results imply that circRNAs are crucial for follicular formation and the estrous cycle, their expression dynamics and regulatory roles in gilts' estrus (ES) and non-ES stages are yet unknown. Our

Accepted: April 15, 2025; Online: April 16, 2025; Received: March 18, 2025 Items for the foundation: The China Agriculture Research System (CARS-35-PIG), the National Natural Science Foundation of China (32472878), and the National Key Research and Development Program of China (2022YFD1300303; 2021YFF1000602) provided funding for this work. Each author made an equal contribution to this work. The authors' email addresses are gsyang@nwafu.edu.cn and guiyanchu@nwafu.edu.cn.

Circular SHOC2 leucine rich repeat scaffold protein (circSHOC2), a novel circRNA, was discovered by researchers. It controls the production of GC steroid hormones through the miR-130b-5p/ASH1-like histone lysine methyltransferase (ASH1L) pathway. By serving as molecular sponges for microRNA (miRNA) response elements (MREs), circRNAs control the translation of mRNA by blocking the binding of miRNAs to their target mRNAs (Patop et al., 2019). Functional and transcriptomic investigations revealed that circSHOC2 directly targets miR-130b-5p. While miR-130b-5p has been linked to lipid metabolism (Liu et al., 2020), cell proliferation (Feng et al., 2024), and carcinogenesis (Chen et al., 2018; Zhang et al., 2019), its biological importance in reproductive endocrine function is yet unknown. The necessity to look into downstream effectors mediating its impact on ovarian steroidogenesis is highlighted by this information gap. ASH1L is a direct target of miR-130b-5p and a crucial hub that links upstream regulatory signals to downstream steroidogenic pathways, according to thorough investigations. The histone methyltransferase encoded by ASH1L catalyzes changes specific to H3K36 (Miyazaki et al., 2013) and plays a role in cell proliferation (Li et al., 2017), cellular differentiation (Xia et al., 2017), and embryonic development (Brinkmeier et al., 2015). Ovarian homeostasis is disturbed by aberrant ASH1L expression: overexpression in mouse oocytes causes apoptosis, reduces primordial follicle pools, and speeds up reproductive senescence (Zhang et al., 2022b), whereas its suppression in cumulus cells hinders proliferation and encourages apoptosis (Cui et al., 2021). These results suggest that ASH1L plays a crucial role in regulating the physiology of female reproduction. Its possible role in the production of steroid hormones is yet unclear, though.

The most significantly differentially expressed transcript in this work was circSHOC2, which was discovered using circRNA sequencing of the ovaries from ES and NES gilts. Functional studies showed that by sponging miR-130b-5p and reducing post-transcriptional regulation of ASH1L, circSHOC2 promotes steroid hormone production in GCs. These findings reveal a molecular connection between noncoding RNA signaling and ovarian endocrine activity and identify circSHOC2 as a hitherto unknown regulator of GC steroidogenic action.

SUPPLIES AND TECHNIQUES

Identification of estrus in gilts

Using mature boars as the major stimulus and BOAR BETTER pheromones (Vetoquinol, France) as an additional cue, New French Yorkshire gilts were exposed to adult boars twice a day for more than 30 minutes each session starting at 160 days of age (McGlone et al., 2023). Individual file cards were used to record timing and behaviors associated to estrus starting at 165 days. External genital alterations, including as vulvar redness, swelling, mucous discharge, and a positive standing reflex, were used to determine estrus

(Yang et al., 2018). Gilts were categorized as non-estrus, in diestrus, or in estrus based on vulvar morphology (Supplementary Figure S1). The lack of quiet estrus or ovarian cysts in NES gilts was verified by postmortem analysis of ovarian morphology, follicular development, and corpus luteum presence (Supplementary Figure S2). Selection of samples and sequencing preparation ES and NES gilt sample selection criteria were adhered to.

procedures developed in earlier research (Shi et al., 2023b). In order to create the core breeding population (C0 generation), 643 healthy, lineage-verified New French Yorkshire sows with at least three parities (average litter size ≥12.5) and at least seven pairs of teats were chosen as the maternal stock at a breeding pig farm in Shaanxi Province. In 102 litters (290 gilts of the C1 generation), estrus was detected at 165 days of age. Gilts that displayed two consecutive estrous cycles were labeled as ES, those that displayed just one estrous cycle as irregular, and those that showed no estrous at all as NES. Of the 102 litters, 32 had irregular estrus patterns, 12 had NES gilts exclusively, and 24 had ES gilts exclusively. Both ES and NES gilts were found in the remaining 34 litters. Out of the 34 litters that satisfied the experimental requirements, we eliminated 4 litters with irregular body condition in order to examine the differences between full-sibling people in estrus and those who are not, eventually choosing 30 litters. One ES gilt and one NES gilt were chosen from the same litter, and the ES gilt was killed during its third estrus. Six groups in all, including six ES gilts and their matching full-sibling NES gilts, were killed. While the left ovaries were utilized for circRNA sequencing, the right ovaries were frozen and kept at -80°C for the purpose of verifying the results of later sequencing. The Northwest Agriculture and Forestry University Committee for the Ethics on Animal Care and Experiments gave its approval to all animal protocols (No. NWAFU-202106025).

Identification and sequencing of CircRNA To create a strand-specific library, ribosomal RNA was eliminated from ovarian tissue samples after total RNA was extracted (Supplementary Table S1). The Illumina NovaSeq™ 6000 platform (USA) was used to prepare the library for sequencing, and the paired-end sequencing read length was 2×150 bp. Adapters and low-quality reads were eliminated from the raw data (Supplementary Table S2). HISAT was utilized to align clean reads to the reference genome Sscrofa11.1 of Sus scrofa (Kim et al., 2015). The gene location data in the genome annotation file (Supplementary Table S3) served as the basis for the analysis. CIRCexplorer2 and CIRI (Gao et al., 2015; Zhang et al., 2016) were used to identify circRNAs. These programs identify circRNAs by analyzing their structural and splicing sequence characteristics. Overlapping the projected circRNA start and end sites allowed for the integration of the prediction results from both methods. Following that, candidate circRNAs were annotated based on their gene connections and genomic positions. CircRNA expression was measured using HTSeq as read counts, which were adjusted for RPM values. It was also established how many splicing site sequences there were (Anders et al., 2015). Porcine ovarian GC primary culture and transfection In accordance with previously established procedures, primary pig GCs were extracted and cultivated (Gao et al., 2023b). Thirty healthy pigs' ovaries were taken from the Yangling Benxiang Group slaughterhouse. After removing the ligaments, the ovaries were incubated in normal saline with 100 U/mL penicillin/streptomycin at 37°C. A 20 mL syringe was used to aspirate follicular fluid containing GCs from healthy follicles that were 3–5 mm in diameter. The suspension was then centrifuged for 10 minutes at 17°C at 800 ×g, and the supernatant was disposed of. 10% fetal bovine serum was added to Dulbecco's Modified Eagle Medium/Nutrient Mixture F-12 (DMEM/F12) to resuspend the cell pellet.

(FBS). Cells were dispersed by repeated pipetting, seeded into culture plates at 10^5 cells/cm^2, and incubated at 37°C in a 5% CO_2 atmosphere. After 24 h, non-adherent cells were removed by washing with phosphate-buffered saline (PBS), and fresh medium was added for continued culture. Cells were subcultured once they reached 50%–60%. After 24 h of transfection, both the culture medium and cells were harvested for further analysis. GCs were transfected using the following reagents: circSHOC2-PCD5 (1 000

ng/mL, Guangzhou Jisai Biotech, China), si-circSHOC2, the miR-130b-5p inhibitor, the miR-130b-5p mimics, and si-ASH1L (50 nmol/L, Shanghai Jima Biotech, China). All reagents were used according to the manufacturer's protocols. Sequence information is provided in Supplementary Table S4. Experimental replicates were set according to the requirements of each assay.

RNA isolation and reverse transcription quantitative PCR (RT-qPCR)

Total RNA was extracted from treated GCs, and expression levels of steroid hormone–related mRNAs were measured using RT-qPCR. cDNA was synthesized from 500 ng of total RNA using the HiScript III RT SuperMix for qPCR (Vazyme, China). RT-qPCR was performed with SYBR PCR mix (Vazyme, China) on a StepOne Real-Time PCR system (ABI, USA). Each reaction contained 25 ng of cDNA and 400 nmol/L primers, with *β-actin* used as the internal control. Relative mRNA expression levels were calculated using the $2^{-\Delta\Delta Ct}$ method. Primer specificity and amplification efficiency ranged from 90% to 110%. Each experimental group included at least three biological replicates and three technical replicates. Primer sequences and RT-qPCR thermal cycling conditions are provided in Supplementary Tables S5, S6.

Western blot analysis

Western blotting was performed with three biological replicates per experimental group. Cultured GCs were lysed using ice- cold radio immunoprecipitation assay (RIPA) protein lysis buffer (Beyotime, China) supplemented with a protease inhibitor (Pierce, USA). Equal amounts of protein (20 μg) were separated using 12% sodium dodecyl sulfate-polyacrylamide gel electrophoresis (SDS-PAGE), with a tri-color prestained protein marker (WJ103, Yamei, China) used to indicate molecular weights. The separated proteins were transferred onto polyvinylidene difluoride (PVDF) membranes (Cell Signaling Technology (CST, USA)) and incubated (4°C, 8h) with the following primary antibodies: anti-cytochrome P450 family 11 subfamily A member 1 (CYP11A1) (ab232763, 60 kDa, 1:1 000, rabbit, Abcam, UK), anti-3β-hydroxy steroid dehydrogenase (3β-HSD) (ab167417, 42 kDa, 1:1 000, rabbit, Abcam), anti-cytochrome P450 family 19 subfamily A member 1 (CYP19A1) (ab106168, 58 kDa, 1:1 000, rabbit, Abcam, UK), anti-steroidogenic acute regulatory protein (StAR) (8449S, 28 kDa, 1:1 000, rabbit, CST, USA), and anti-cytochrome P450 family 17 subfamily A member 1 (CYP17A1) (ab125022, 55 kDa, 1:1000, rabbit, Abcam, UK). β-ACTIN (sc-47778, 43 kDa, 1:1 000, mouse, Santa Cruz, USA) was used as a loading control. Subsequently, the membranes were incubated (17°C, 2h) with horseradish peroxidase (HRP)-conjugated secondary antibodies: mouse anti-rabbit immunoglobulin G (IgG) (sc- 2357, 1:5 000, Santa Cruz, USA) and goat anti-mouse IgG (sc-2005,1:5000,SantaCruz,USA).Proteinsignalswere detected using the iBright 1500 system (Thermo Fisher Scientific, USA) and quantified with ImageJ software (http://imagej.nih.gov/ij/).Luciferase reporter assay

Luciferase reporter plasmids (psi-CHECK2) containing wild- type circSHOC2 (circSHOC2-WT), mutant circSHOC2 (circSHOC2-Mut), wild-type 3' untranslated region (3'UTR) of ASH1L (ASH1La-WT), and mutant 3'UTR of ASH1L (ASH1Lb- Mut) were constructed by General Biosystems (China). Sequence information of all WT and mutant constructs is shown in Supplementary Table S7. HEK293T cells were seeded in 48-well plates, and cotransfected with WT or MUT 3 ′UTR luciferase reporter plasmids, along with miRNA mimics or negative control, using Lipofectamine 2000 (Thermo Fisher Scientific, USA). After 24 h of transfection, the cells were harvested, and luciferase activity was quantified using the Dual- Glo Luciferase Assay System (Promega, USA) according to the manufacturer's instructions. Firefly luciferase activity was used for normalization. Each experimental group included three biological replicates.

Enzyme-linked immunosorbent assay (ELISA)

E_2 levels were measured using a porcine E_2 ELISA kit (YJ002366, Yuanju Biotechnology Center, China) following the manufacturer's

instructions. The kit exhibited intra-assay and inter-assay coefficients of variation (CV) below 10% and 15%, respectively, and a sensitivity range of 2.5–200 pg/mL. P_4 levels were measured with a porcine P_4 ELISA kit (YJ002422, Yuanju Biotechnology Center, China), with an intra-assay CV < 10%, inter-assay <15%, and a sensitivity range of 0.625–20 ng/ mL. Absorbance was recorded at 450 nm using a Multiskan™ FC spectrophotometer (Thermo Fisher Scientific, USA). Both kits employed monoclonal antibodies with no cross-reactivity. Each experimental group included four biological replicates.

Bioinformatics analysis

Potential miRNAs targeting circSHOC2 were predicted using TargetScan (http://www.targetscan.org) and miRanda (http://mirtoolsgallery.tech/mirtoolsgallery/node/1055). Candidate target genes of miR-130b-5p were identified using TargetScan (http://www.targetscan.org), miRDB (http://mirdb. org/), and miRwalk (http://mirwalk.umm.uni-heidelberg.de/). Predictions were made by inputting the sequences and gene names of circSHOC2 and miR-130b-5p and selecting appropriate species. RNAhybrid (https://bibiserv.cebitec.uni-bielefeld.de/rnahybrid/) was used for sequence binding analysis and free energy prediction of target genes. Gene Ontology (GO) and Kyoto Encyclopedia of Genes and Genomes (KEGG) pathway analyses were performed via KOBAS v.3.0 (http://kobas.cbi.pku.edu.cn/index.php).

RNase R digestion assay

Each experimental group included three biological replicates. Total RNA was extracted from GCs and incubated with the RNase R digestion kit (RNR07250, Epicentre Biotechnologies, USA) at 37℃ for 30 min to selectively degrade linear RNA while preserving circRNA. The resulting RNA was reverse transcribed and amplified by RT-qPCR. Amplification products were assessed by gel electrophoresis to confirm circRNA resistance to RNase R digestion.

Cytoplasmic and nuclear RNA purification

Each experimental group included three biological replicates. Cytoplasmic and nuclear RNA were isolated using the Cytoplasmic and Nuclear RNA Purification Kit (CH-21000, Norgen BioTek, Canada). Briefly, GC suspensions were centrifuged at 1000 ×*g* for 10 min at 4°C, lysed with lysis buffer, and separated into cytoplasmic (supernatant) and nuclear(pellet) fractions by centrifugation (20 000 ×*g* for 10 min at 4°C). Each fraction was mixed with buffer and ethanol, transferred to a spin column, washed, and eluted. Purified RNA was stored at −80℃ for downstream applications.

Statistical analysis

Experimental data were analyzed using GraphPad Prism v8 (https://www.graphpad-prism.cn/). Results are presented as mean±standard error of the mean (SEM) based on at least three biological replicates. Comparisons between two groups were performed via two-tailed unpaired Student's *t*-tests. Comparisons involving three or more groups were determined using one-way or two-way analysis of variance (ANOVA), followed by Dunnett and Sidak *post hoc* tests, respectively. Statistical significance was denoted as ns: Not significant; *: P<0.05; **: P<0.01; ***: P<0.001; ****: P<0.0001.

RESULTS

Identification and differential profiling of ovarian circRNAs in ES and NES gilts

New French Yorkshire gilts with a shared genetic background and identical feeding conditions were categorized into the ES and NES groups following standardized estrus detection protocols (Figure 1A). Morphological examination of reproductive organs revealed that NES gilts exhibited smaller ovaries and uteri, with no visible mature follicles or corpora lutea (Figure 1B, C). Serum E_2 and P_4 levels were significantly lower in the NES group compared to the ES group (Figure 1D), confirming the absence of silent estrus and validating the selection criteria for transcriptomic analysis.

High-throughput circRNA sequencing of

ovarian tissue, followed by systematic bioinformatic analysis, identified 17 662 distinct circRNAs across all samples, including 3 919 present in both the NES and ES groups (Figure 1E, F). Host gene annotation revealed 5 275 protein-coding genes, with 2 846 shared between groups, representing 54.0% of all host genes (Figure 1G, H). Notably, 37.18% of the genes produced a single circRNA, while the remaining genes generated two or more circRNAs (Figure 1I). Chromosomal mapping demonstrated genome-wide circRNA distribution, with pronounced density on chromosome 12. Most circRNAs spanned multiple genomic regions, with only a small fraction originating from a single exon, intron, or intergenic region (Figure 1J).

Further analysis identified 67 differentially expressed circRNAs (DECs) between the ES and NES groups ($-\log_{10}$ (*P*-value)>1.301, $|\log_2$(fold change)|>1) (Supplementary Table S8), including 30 up-regulated and 37 down-regulated candidates (Figure 2A, B). Chromosomes 1 and 6 harbored the highest number of DECs (Figure 2C). Notably, the *CUL1* gene encoded two significantly up-regulated circRNAs (circRNA1422 and circRNA1794) in ES ovaries, while all other host genes encoded only a single circRNA.

Cross-referencing with public circRNA databases revealed that 55 DECs originated from annotated host genes, while 11 mapped to intergenic regions. GO enrichment analysis indicated functional association of host genes with the Arp2/3 protein complex, mRNA processing body assembly, ubiquitin ligase complex, RNA phosphodiester bond hydrolysis, and regulation of estradiol secretion (Figure 2D). KEGG pathway analysis further highlighted enrichment in pathways related to TGF-β signaling, ECM-receptor interaction, actin regulation, and p53 signaling (Figure 2E). To validate sequencing-based differential expression profiles, six circRNAs were selected for RT-qPCR. All six circRNAs exhibited expression trends consistent with the high-throughput sequencing data. Among them, circ1855 showed the highest fold change and was derived from the *SHOC2* gene. This circRNA was subsequently designated as circSHOC2 (Figure 2F, G).

Overall, circRNA transcriptome profiling of ES and NES gilts yielded a comprehensive ovarian circRNA atlas and identified circSHOC2 as a key differentially expressed transcript potentially linked to estrous regulation.

CircSHOC2 promotes steroid hormone synthesis in GCs CircSHOC2 was generated via back-splicing of exon 4 of the *SHOC2* gene and spanned 943 base pairs in length (Figure 3A), with RNase R digestion confirming a stable circular structure (Figure 3B, C). RT-qPCR revealed significantly higher expression of circSHOC2 in ES ovaries relative to NES ovaries (Figure 3D). Subcellular fractionation further indicated predominant localization of circSHOC2 in the cytoplasmic compartment of GCs (Figure 3E), suggesting a post-transcriptional regulatory role.

Functional assays in primary porcine GCs revealed that silencing circSHOC2 with si-circSHOC2 significantly suppressed its expression (Figure 3F), leading to a marked reduction in E_2 and P_4 concentrations in the culture supernatant compared with the control group (Figure 3G). Concomitantly, both mRNA and protein levels of key steroidogenic genes, including *CYP11A1*, *CYP19A1*, and *3β-HSD*, were also substantially reduced following circSHOC2 knockdown (Figure 3H−J). In contrast, overexpression of circSHOC2 through the circSHOC2-PCD5 vector (Figure 3K) resulted in elevated steroid hormone levels (Figure 3L), accompanied by significant up-regulation of CYP11A1, CYP19A1, and 3β-HSD at both transcript and protein levels (Figure 3M−O). Collectively, these findings suggest that circSHOC2 plays a role in promoting steroid hormone synthesis in porcine GCs by modulating the expression of key enzymes involved in steroidogenic pathways.

CircSHOC2 modulates steroidogenesis in GCs through direct interaction with miR-130b-5p

To elucidate the regulatory mechanism by which circSHOC2 influences steroid hormone biosynthesis in GCs, miRNAs potentially

targeted by circSHOC2 were predicted using TargetScan and miRanda online tools (Figure 4A). Integration of these predictions with miRNA sequencing (miRNA-seq) data from ES and NES ovaries, followed by expression profiling and seed sequence complementarity analysis, highlighted miR- 130b-5p as a high-confidence target. Quantitative analysis revealed significantly lower expression of miR-130b-5p in ES ovaries compared to NES ovaries (Figure 4B). Binding site prediction confirmed a complementary interaction between miR- 130b-5p and circSHOC2, with a calculated binding free energy of −22.4 kcal/mol (Figure 4C).

Dual-luciferase assays were performed using psiCHECK2 constructs carrying WT or mutated circSHOC2 binding sites (circSHOC2-WT and circSHOC2-Mut, respectively; Figure 4D). Overexpression of miR-130b-5p significantly reduced luciferase activity of circSHOC2-WT but had no effect on circSHOC2- Mut activity, confirming that miR-130b-5p is a direct target of circSHOC2 (Figure 4E). Additionally, co-transfection of circSHOC2-PCD5 with miR-130b-5p mimics significantly increased miR-130b-5p levels compared with the control (circSHOC2-PCD5+mimics NC) (Figure 4F).

Inhibition of miR-130b-5p in primary ovarian GCs led to a

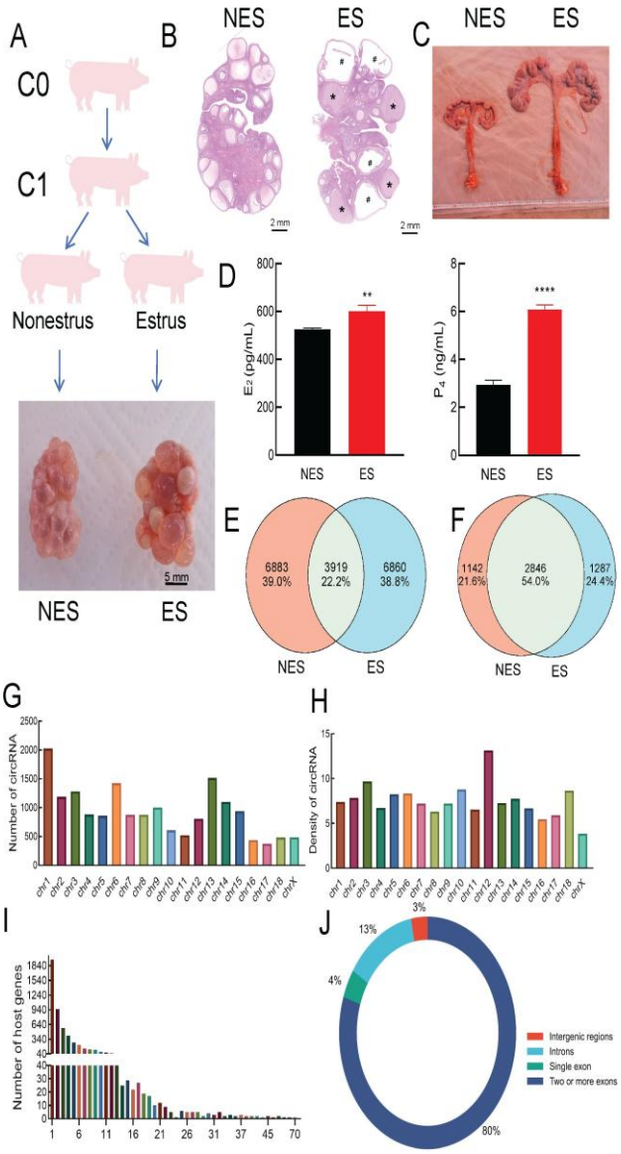

Figure 1 CircRNA expression profiles in ovaries of ES and NES gilts

A: Selection process for ES and NES ovarian samples. B: Representative H&E-stained ovarian sections from NES and ES groups; scale bars, 2 mm. #: Large follicle; *: Corpus luteum. C: Representative uterine morphology in NES and ES groups. D: Serum concentrations of E_2 and P_4. **: $P<0.01$; ****: $P<0.0001$. E: Number of circRNAs identified in ES and NES ovaries. F: Number of host genes associated with circRNAs. G: Number of circRNAs identified on each chromosome. H: Distribution density of circRNAs across chromosomes, expressed as number of circRNAs per megabase (Mb) of chromosome length. I: Number of circRNAs produced by host genes. J: Composition analysis of circRNAs, indicating proportions derived from multiple

exons, single exons, single introns, and intergenic regions.

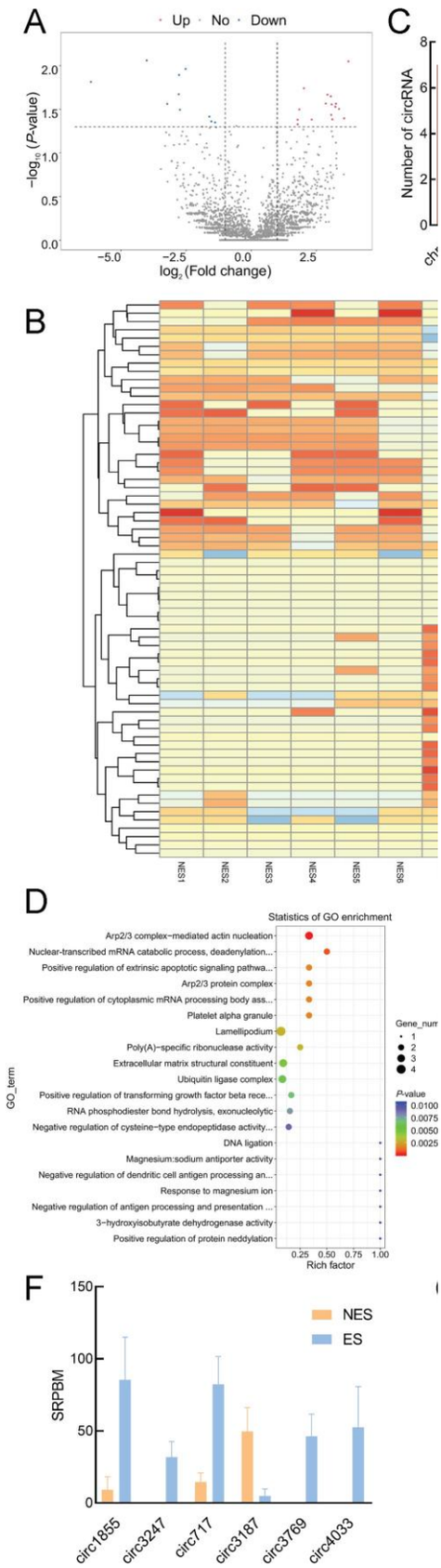

Figure 2 Functional annotation and validation of host genes of differentially expressed circRNAs

A: Volcano plot showing differentially expressed circRNAs. B: Heatmap showing expression profiles of differentially expressed circRNAs. C: Chromosomal locations of differentially expressed circRNAs. D: Bar chart showing GO enrichment analysis results. E: Bubble chart showing top 20 KEGG enriched pathways. F: Expression levels of circRNAs identified through sequencing in ES and NES ovaries. G: Validation of circRNA expression in ES and NES ovaries by RT-qPCR, n=6. *: P<0.05.

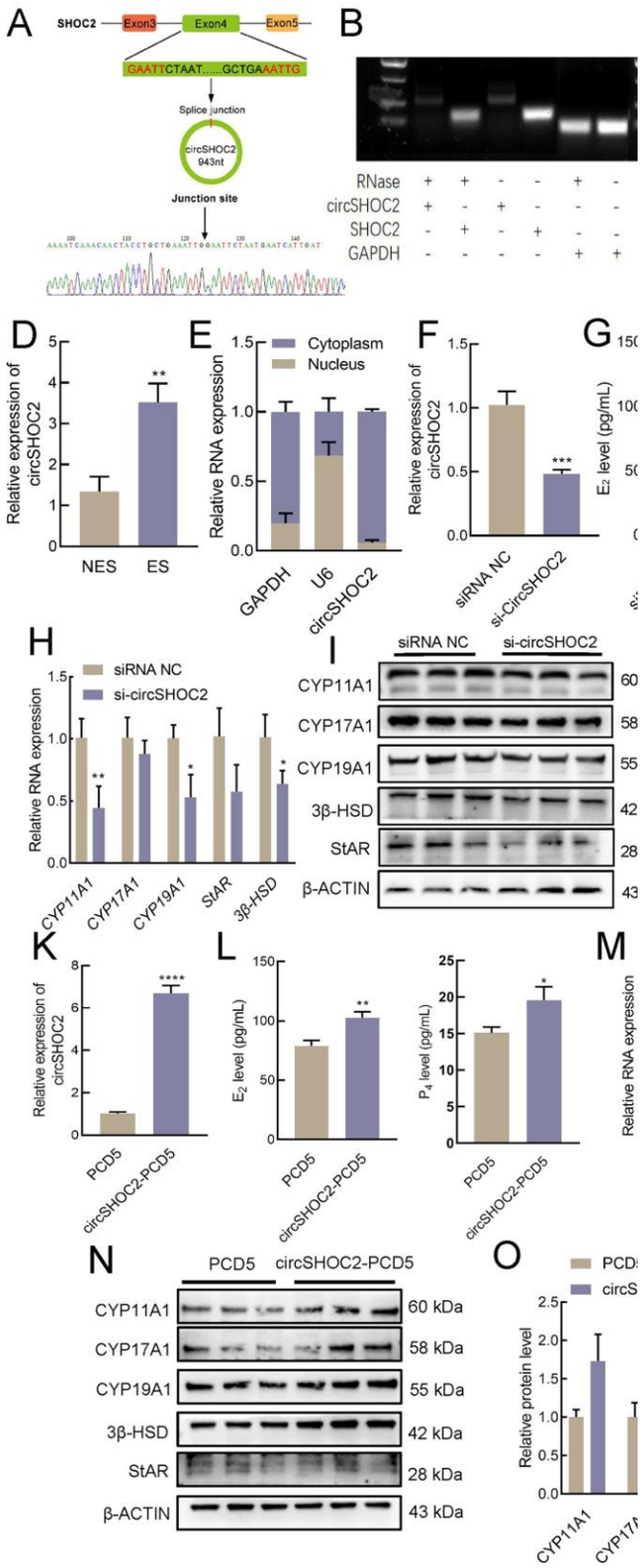

Figure 3 Effect of circSHOC2 on steroid hormone synthesis in ovarian GCs

A: Schematic representation of circSHOC2 structure. B: Detection of circSHOC2 and SHOC2 mRNA following RNase R digestion, *n*=3. C: RT- qPCR product electrophoresis following RNase R digestion, *n*=3. D: Validation of circSHOC2 expression in ovarian tissues from ES and NES sows by RT-qPCR, *n*=6. E: RNA detection of circSHOC2 in nuclear and cytoplasmic fractions, *n*=5. F: Efficiency of circSHOC2 knockdown, *n*=5. G: Concentrations of E_2 and P_4 in supernatants based on ELISA, *n*=4. H: mRNA expression levels of genes related to steroid hormone synthesis based on RT-qPCR, *n*=4. I, J: Protein expression levels of steroid hormone synthesis-related genes based on western blot analysis, *n*=3. K: Efficiency of circSHOC2 overexpression, *n*=5. L: Concentrations of E_2 and P_4 in supernatants based on ELISA, *n*=4. M: mRNA expression levels of genes related to steroid hormone synthesis based on RT-qPCR, *n*=4. N, O: Protein expression levels of steroid hormone synthesis-related genes based on western blot analysis, *n*=3. *: $P<0.05$; **: $P<0.01$; ***: $P<0.001$; ****: $P<0.0001$.

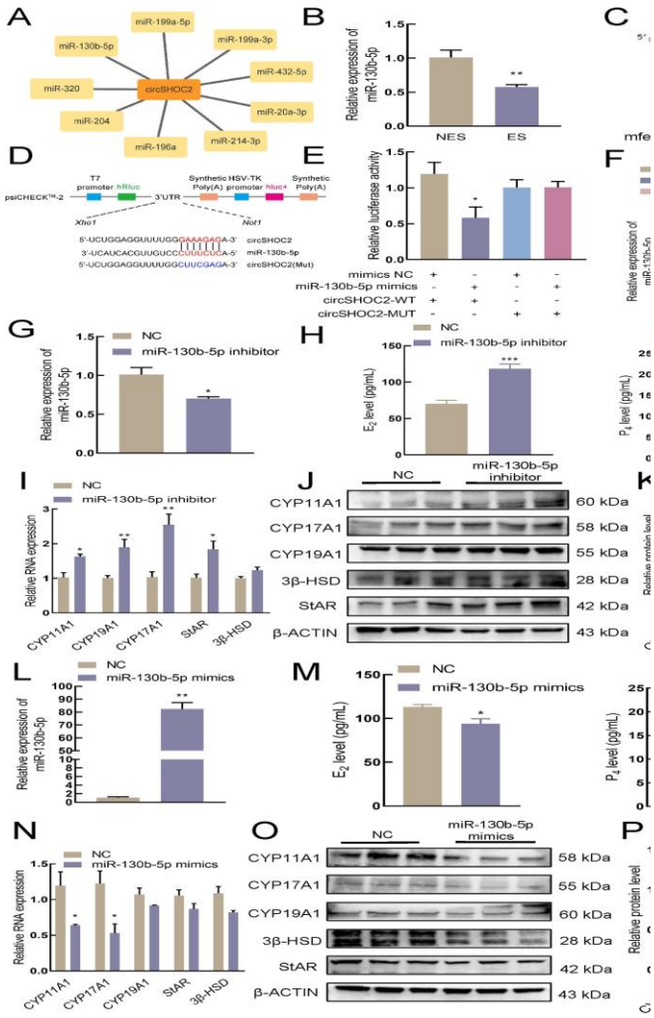

Figure 4 CircSHOC2 sponges miR-130b-5p to regulate steroid hormone synthesis in GCs

A: Predicted miRNA network targeted by circSHOC2. B: RT-qPCR analysis showing miR-130b-5p mRNA expression in ES and NES ovarian tissues, *n*=4. C: Prediction of circSHOC2-miR-130b-5p binding sites. D: Schematic of dual-luciferase reporter vector. E: Results of dual-luciferase reporter assay, *n*=3. F: mRNA expression level of miR-130b-5p following circSHOC2 overexpression and circSHOC2 and miR-130b-5p overexpression, *n*=3. G: Efficiency of miR-130b-5p inhibitor suppression, *n*=4. H: Concentrations of E_2 and P_4 based on ELISA, *n*=6. I: RT-qPCR analysis of steroid hormone synthesis-related gene mRNA expression, *n*=4. J, K: Western blot analysis of steroid hormone synthesis-related protein expression, *n*=3. L: Efficiency of miR-130b-5p mimic overexpression, *n*=4. M: Concentrations of E_2 and P_4 based on ELISA, *n*=6. N: RT-qPCR analysis of steroid hormone synthesis-related gene mRNA expression, *n*=4. O, P: Western blot analysis of steroid hormone synthesis-related protein expression, *n*=3. *: $P<0.05$; **: $P<0.01$; ***: $P<0.001$. significant reduction in miR-130b-5p expression (Figure 4G), accompanied by marked increases in the concentrations of E_2 and P_4 compared to the control group (Figure 4H). Interference with miR-130b-5p significantly increased the mRNA levels of *CYP17A1*, *CYP19A1*, *CYP11A1*, and *StAR*, as well as the protein levels of CYP11A1, CYP17A1, StAR, and 3β-HSD (Figure 4I, J, L). Conversely, primary GC treatment with miR-130b-5p mimics exerted the opposite effects (Figure 4L), reducing steroid hormone content and the expression of related genes (Figure 4M–P). These findings indicate that miR-130b- 5p inhibits the synthesis of E_2 and P_4 in GCs.

Rescue assays revealed that concurrent overexpression of circSHOC2 and miR-130b-5p attenuated circSHOC2-mediated enhancement of steroid hormone production in GCs (Supplementary Figure S3A–C), confirming that circSHOC2 promotes steroidogenesis, at least in part, through sequestration of miR-130b-5p.

CircSHOC2-miR-130b-5p-ASH1L axis modulates steroid hormone synthesis in GCs

Given the conservation of the miR-130b-5p binding site on circSHOC2 across humans, mice, and pigs (Figure 5A), the miRDB, miRWalk, and TargetScan databases were used to predict the target genes of miR-130b-5p. Cross-database analysis yielded 27 candidate genes (Figure 5B). Among these, ASH1L was prioritized based on ovarian expression levels, literature relevance, complete 3'UTR complementarity to the miR-130b-5p seed sequence, favorable binding free energy (−31.0 kcal/mol), and dual-luciferase reporter assay validation (Figure 5C, D). Inhibiting miR-130b-5p increased ASH1L expression, while miR-130b-5p mimics inhibited ASH1L expression (Supplementary Figure S3D, E). Dual-luciferase

assays in HEK293T cells confirmed direct regulation of ASH1L by miR-130b-5p. Cotransfection with miR-130b-5p mimics significantly suppressed luciferase activity from one WT ASH1L 3'UTR construct, while no significant change was observed for the other WT construct or mutant version lacking the miR-130b-5p binding site (Figure 5E). These findings demonstrate that ASH1L is a direct target of miR-130b-5p, with regulation dependent on a specific seed-binding site.

To explore the role of ASH1L in steroidogenesis, siRNA- mediated knockdown was performed in porcine GCs (Figure 5F). Compared with the siRNA NC, silencing ASH1L resulted in a significant reduction in E_2 and P_4 secretion (Figure 5G, H). Additionally, the mRNA levels of *CYP11A1*, *CYP17A1*, *CYP19A1*, and *3β-HSD* were significantly reduced, as were the protein levels of CYP17A1 and 3β-HSD (Figure 5I −K). Rescue experiments confirmed that co-transfection of the miR-130b-5p inhibitor with si-ASH1L restored E_2 and P_4 concentrations otherwise suppressed by ASH1L knockdown (Figure 5L–N). Additionally, coexpression of circSHOC2-PCD5 and miR-130b-5p mimics significantly reduced ASH1L expression compared to the control (circSHOC2-PCD5+mimics NC) (Supplementary Figure S3F), indicating that circSHOC2 modulates ASH1L levels through miR-130b-5p sequestration.

DISCUSSION

Comprehensive profiling of porcine ovarian circRNAs has previously revealed expression differences across estrous stages (Niu et al., 2022), between animals with divergent reproductive capacities (Liang et al., 2020), and during physiological processes such as ovarian aging (Xi et al., 2019) and follicular atresia (Guo et al., 2020). However, circRNA landscapes in ES and NES gilts remain unexplored.

In the present study, 5 275 host genes were identified from ovarian circRNAs in ES and NES gilts. Pathway enrichment analysis revealed significant association with TGF signaling, ECM-receptor interaction, actin regulation, and p53 signaling pathways. These pathways are functionally integral to GC physiology. Notably, TGF signaling regulates GC proliferation, apoptosis, and estrogen biosynthesis (Bai et al., 2017; Lundberg et al., 2022); actin remodeling plays a critical role in regulating steroidogenic output (Chen et al., 2023); and p53 signaling governs apoptotic responses in GCs (Joo et al., 2023). These findings suggest that ovarian circRNAs may influence estrous expression by modulating GC survival and steroid hormone synthesis.

The synthesis of steroid hormones represents a fundamental role of ovarian GCs (Bjersing et al., 1964), and accumulating evidence supports a regulatory role for circRNA in this process. For example, circDDX10 expression, which declines with age in human ovaries, inhibits E_2 synthesis when silenced, concomitant with down-regulation of steroidogenic genes (Cai et al., 2021). Similarly, circRPS19, which exhibits differential expression during chicken follicular development, promotes GC proliferation and steroidogenesis via the miR-218-5p/INHBB axis (Wei et al., 2024). In the present study, circSHOC2 emerged as the most significantly differentially expressed circRNA between ES and NES gilts and was subsequently shown to regulate steroidogenesis in GCs by modulating CYP19A1, StAR, and 3β-HSD expression, thereby enhancing E_2 and P_4 synthesis.

CircRNAs typically regulate cellular processes by functioning as competing endogenous RNAs (ceRNAs) that sequester specific miRNAs. For example, circ0001470 promotes embryonic development by sponging miR-140-3p and modulating PTGFR expression (Zhang et al., 2022a), while circKDM5B enhances porcine blastocyst development by regulating trophoblast barrier function through sponging miR- 128 (Gao et al., 2023a). In the current study, miR-130b-5p— abundantly expressed in the ovaries of NES gilts—was identified as a direct target of circSHOC2. Previous studies have shown that miR-130b-5p regulates cell proliferation (Zhang et al., 2019) and lipid metabolism (Feng et al., 2024), and that miR-130a-5p can be sponged by circWHSC1 (Shi et al., 2023a). These findings suggest that miR-130b-5p may similarly regulate the cellular state of GCs, thereby

affecting cell function. Here, dual-luciferase assays confirmed the interaction between miR-130b-5p and circSHOC2, and rescue experiments demonstrated that circSHOC2 promotes E_2 and P_4 synthesis in GCs through miR-130b-5p sequestration. These results provide the first evidence that miR-130b-5p directly regulates steroid hormone biosynthesis in porcine GCs.

ASH1L was identified as a downstream target

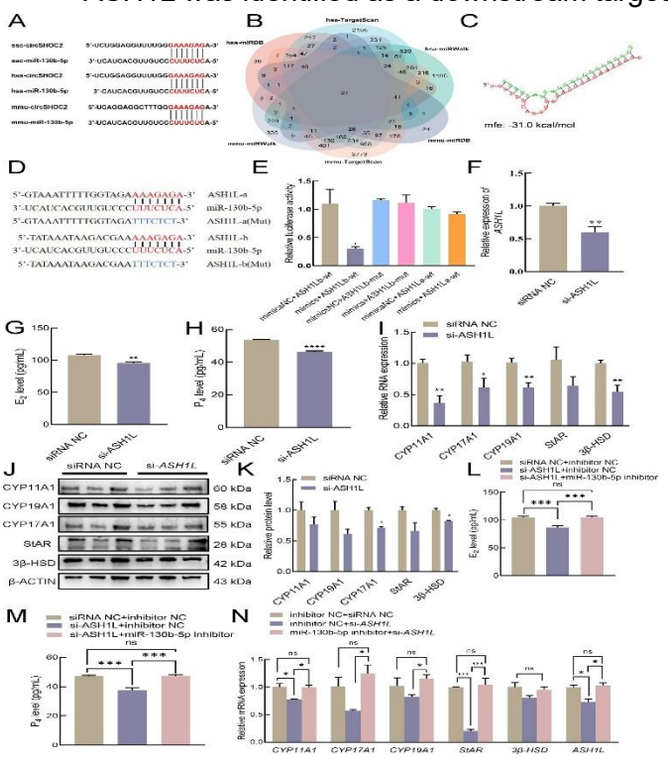

of miR-130b- 5p through integrative miRNA target prediction. ASH1L functions as a key epigenetic regulator (Xi et al., 2020), with evidence from bovine cumulus cells indicating that its knockdown can significantly suppress cell proliferation, promote apoptosis, and reduce H3K36me1/2/3 methylation (Cui et al., 2021). Although the direct involvement of H3K36 methylation in regulating steroidogenic enzymes remains unclear, ASH1L is known to colocalize with H3K4me3 and modulate histone methylation dynamics (Vann et al., 2025). Furthermore, epigenetic studies have identified functional H3K4me3 regulatory elements in the promoter regions of key steroidogenic genes, including CYP19A1 (Madogwe et al.,

Figure 5 MiR-130b-5p targets and inhibits ASH1L to regulate steroid hormone synthesis in GCs

A: Binding sites of circSHOC2 and miR-130b-5p in humans, mice, and pigs. B: Screening for target genes via multiple databases. C: Prediction of binding sites. D: Schematic of two ASH1L dual-luciferase reporter vectors. E: Dual-luciferase activity assay. F: Inhibition efficiency of si-ASH1L, *n*=3. G: Concentration of E_2 based on ELISA, *n*=4. H: Concentration of P_4 based on ELISA, *n*=4. I: mRNA expression levels of steroid hormone synthesis-related genes based on RT-PCR, *n*=4. J, K: Protein expression levels of steroid hormone synthesis-related genes based on western ^{blot} analysis, *n*=3. L: Concentration of E_2 based on ELISA, *n*=5. M: Concentration of P_4 based on ELISA, *n*=5. N: mRNA expression levels of steroid hormone synthesis-related genes, *n*=3. ns: Not significant; *: P<0.05; **: P<0.01; ***: P<0.001; ****: P<0.0001. ssc: *Sus scrofa*; hsa: *Homo sapiens*; mmu: *Mus musculus*.

Figure 6 Schematic model illustrating how circSHOC2, identified

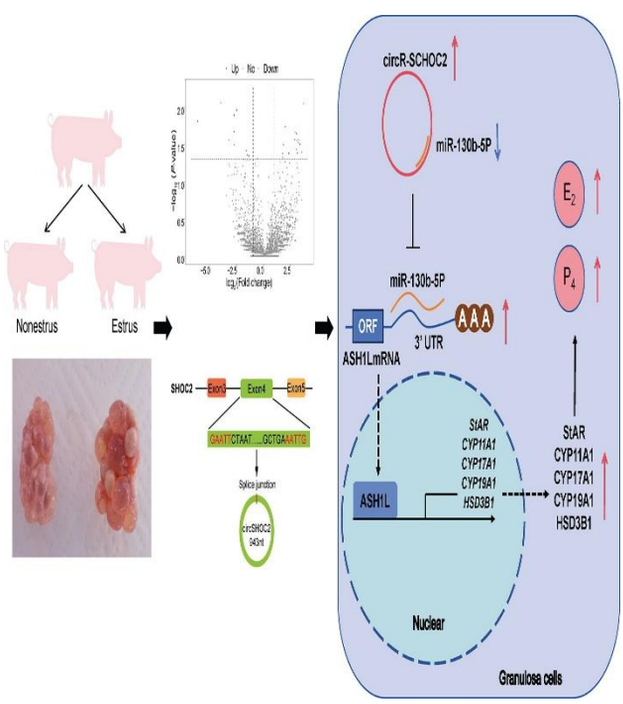

2020), CYP11A1 (Okada et al., 2016), and StAR (Li et al., 2024). These findings suggest that

ASH1L may regulate steroidogenesis by modulating H3K4me3 modifications. However, the mechanistic link between ASH1L-mediated histone modification and transcriptional regulation of steroidogenic pathways remains unresolved and will be the focus of future investigations.

While estrus regulation involves a complex molecular network, this study specifically examined the function of circSHOC2 in GCs. Ongoing work will aim to characterize additional circRNAs, expand the ceRNA interaction landscape, and refine the regulatory architecture governing steroid hormone biosynthesis in porcine ovaries

In summary, this study identified circSHOC2 as a key regulatory circRNA that regulates the synthesis of E_2 and P_4 in ovarian GCs via the circSHOC2/miR-130b-5p/ASH1L axis, offering novel insights into the molecular regulation of reproductive function in replacement gilts.

CONCLUSION

CircRNA sequencing of ovarian tissues from ES and NES gilts identified circSHOC2 as a differentially expressed circRNA that regulates the synthesis of E_2 and P_4 in ovarian GCs via the circSHOC2/miR-130b-5p/ASH1L axis (Figure 6).

DATA AVAILABILITY

The datasets used and analyzed in the current study are available from the corresponding author upon reasonable request. The raw RNA-seq data analyzed in this study are available from the China National Center for Bioinformation database of the Genome Sequence Archive (GSA) REFERENCES

Am-In N, Suwimonteerabutr J, Kirkwood RN. 2020. Serum anti-mullerian hormone and estradiol concentrations in gilts and their age at puberty. *Animals*, **10**(11): 2189.

Anders S, Pyl PT, Huber W. 2015. HTSeq—a Python framework to work with high-throughput sequencing data. *Bioinformatics*, **31**(2): 166–169.

Bai L, Chu GY, Wang WS, et al. 2017. BAMBI promotes porcine granulosa cell steroidogenesis involving TGF-β signaling. *Theriogenology*, **100**: 24–31.

Bjersing L, Cartensen H. 1964. The role of the granulosa cell in the biosynthesis of ovarian steroid hormones. *Biochimica et Biophysica Acta (BBA) - General Subjects*, **86**(3): 639–640.

Brinkmeier ML, Geister KA, Jones M, et al. 2015. The histone methyltransferase gene absent, small, or homeotic discs-1 like is required for normal hox gene expression and fertility in mice. *Biology of Reproduction*, **93**(5): 121.

Cai HC, Chang TL, Li YM, et al. 2021. Circular *DDX10* is associated with ovarian function and assisted reproductive technology outcomes through modulating the proliferation and steroidogenesis of granulosa cells. *Aging*, **13**(7): 9592–9612.

Chen D, Wu CQ, Wei SM, et al. 2023. Semaphorin 4C regulates ovarian steroidogenesis via actin cytoskeleton reorganization mediated by RHOA/ROCK1. Gaad010 in Molecular Human Reproduction, 29(5).

Yang YQ, Wang J, Chen H, et al. (2018). By targeting RASAL1, miR-130b-5p encourages the growth, migration, and invasion of gastric cancer cells. Letters on Oncology, 15(5): 6361–6367.

Hao HS, Cui LX, Tian YQ, et al. 2021. In bovine cumulus cells, ASH1L methyltransferase knockdown caused apoptosis, which inhibited proliferation and H3K36 methylation. 65–73 in Theriogenology, 161.

Bevier GW, Dial GD, Dial OK, et al. 1983. The prepubertal gilt's diurnal luteinizing hormone release and estrous behavior in response to exogenous estrogen. Reproduction Biology, 29(5): 1047–1056.

Hernandez LL, Wiltbank MC, and Domingues RR. 2023. The antidepressant fluoxetine (Prozac®) changes mice's estrous cycles and modifies uterine estrogen signaling. Endocrinology, Molecular and Cellular, 559: 111783. Li JG, Wu YK, Feng K, et

al. 2024. Mir-130b-5p plays a crucial function in the proliferation of cardiomyocytes and the healing of the heart in mice following myocardial infarction. 29–41 in Stem Cells, 42(1).
DeVore AA, Perego MC, Feng T, et al. 2019. N-carbamylglutamate and arginine's effects on the in vitro steroidogenesis and proliferation of pig granulosa cells. Science of Animal Reproduction, 209: 106138.
Liu JB, Jiang H, Fu Y, et al. 2018. Circular RNAs throughout the genome of bovine cumulus cells treated with BMP15 and GDF9. 7944 in Scientific Reports, 8(1).
Yang YL, Gao D, Wang X, et al. 2023a. Porcine blastocyst development is regulated by CircKDM5B sponges miR-128, which alter trophectoderm barrier function. gaad027 in Molecular Human Reproduction, 29(9).
Zhang LT, Gao L, Zhang YL, and others (2023b). MiR-10a-5p targets CREB1 and suppresses cholesterol metabolism to prevent the formation of steroid hormones in pig granulosa cells. 19–29 in Theriogenology, 212.
Gao Y, Zhao FQ, and Wang JF. 2015. CIRI: a de novo circular RNA identification algorithm that is impartial and effective. 16(1), Genome Biology: 4.
Lucas CG, Geisert RD, Bazer FW, et al. 2024. Pig mothers use prostaglandins, cytokines, and sex hormones as part of a servomechanism to detect pregnancy. Science of Animal Reproduction, 264: 107452.
Huang L, Yao W, Guo TY, et al. 2020. Circular RNAs' possible biological roles at the onset of atresia in pig follicles. 72: 106401 in Domestic Animal Endocrinology.
Wang K, Jeck WR, Sorrentino JA, et al. (2013). ALU repetitions are linked to circular RNAs, which are plentiful and conserved. 19(2): 141–157 in RNA.
Wu J, Xu B, and Jia WC. 2018. Circular RNA epidermal growth factor receptor function in granulosa cells and circular RNA expression profiles of mouse ovaries during postnatal development. Metabolism, 85: 192-204.
Park SA, Park JH, Joo NR, et al. 2023. By controlling SIRT1/p53, TOPK prevents granulosa cell apoptosis caused by TNF-α. Communications for Biochemical and Biophysical Research, 664: 128–135.
Salzberg SL, Kim D, and Langmead B. 2015. A quick spliced aligner with minimal memory needs is called HISAT. 357–360 in Nature Methods, 12(4).
Knox RV, 2024. Climate change and swine fecundity. Science of Animal Reproduction, 269: 107537.
Medvedova M, Halenar M, Kolesarova A, et al. (2017). the impact of zearalenone and deoxynivalenol on the in vitro synthesis of steroid hormones by pig ovarian granulosa cells. 52(11): 823–832 in Journal of Environmental Science and Health, Part B.
Soede NM, Langendijk P, van den Brand H, et al. 2000. impact of boar contact on the development of follicles and the expression of estrus in primiparous sows following weaning. 1295–1303 in Theriogenology, 54(8).
Yang R, Lu L, Li FP, et al. 2024. Comparative steroidogenic effects of perfluorooctanoic acid (PFOA) and hexafluoropropylene oxide trimer acid (HFPO-TA): Control of histone alterations. 350: 124030; Environmental Pollution.
Ye ZS, Shi C, Li G, et al. (2017). In mice, epidermal homeostasis depends on the histone methyltransferase ash1l. Reports on Science, 7: 45401.
Guo J, Yan JY, Liang GM, et al. 2020. Ovarian circular RNAs were identified, and MeiShan and huge white pigs' differential expression was examined. Basel, Animals, 10(7): 1114.
Yang YL, Niu GL, Liang GM, et al. (2017). Sus scrofa circular RNA genome-wide profiling in three developmental stages and nine organs. 523–535 in DNA Research, 24(5).
Zhang CL, Chen JH, Liu MZ, et al. 2024. Transcriptome study and characterization of several pig tissues during estrus and diestrus. Journal of Biological Macromolecules International, 256: 128324.
Zhang LJ, Liu XN, and Chen SH. 2020. Insulin resistance and lipid buildup are prevented in a mouse model of nonalcoholic fatty liver disease by downregulating microRNA-130b-5p. Endocrinology and Metabolism in the American Journal of Physiology, 319(1): E34–E42.
Maucieri AM, Lundberg AL, Jaskiewicz NM, et al. 2022. TGFα stimulates granulosa cells in tiny antral follicles in cows. Skac105, Journal of Animal Science, 100(7).
Wu WZ, Ma BC, Wang SH, et al. 2023.

CircRNA/lncRNA-miRNA interaction mechanisms and their uses in pharmacological and illness research. Pharmacotherapy & Biomedicine, 162: 114672.
Tanwar DK, Taibi M, Madogwe E, et al. 2020. Global examination of histone modification and FSH-regulated gene expression in mouse granulosa cells. 1082–1096 in Molecular Reproduction and Development, 87(10).
Sanchez M, McGlone JJ, Duke L, et al. 2023. In gilts who are not exposed to boars, self-administration of a boar priming pheromone induces puberty. Basel, Animals, 14(1): 91.
Yada Y, Miyazaki H, Higashimoto K, et al. (2013). Ash1l counteracts polycomb silencing by methylating histone H3's Lys36 without the aid of transcriptional elongation. e1003897 in PLoS Genetics, 9(11).
Huang YL, Lu H, Niu X, et al. 2022. CircRNAs in the diestrus and estrous phases of Xiang pig ovaries. 8(1): 29 in Porcine Health Management.
In 2016, Okada M, Lee L, Maekawa R, et al. During ovulation in female rats, granulosa cells undergoing luteinization undergo epigenetic modifications of the cyp11a1 promoter region. 3344–3354 in Endocrinology, 157(9).
In 2019, Patop IL, Wě S, and Kadener S. CircRNAs: their history, present, and future. e100836 in The EMBO Journal, 38(16).
Swan CL, Crellin NK, Rodway MR, et al. 1999. Progestins play a part in the steroid control of progesterone production in a stable porcine granulosa cell line. Molecular Biology and Steroid Biochemistry Journal, 68(5): 173–180.
Liu X, Shi L, Zhao YS, et al. 2023a. Circular RNA circWHSC1 targets miR-130a-5p/zeb1 signaling in vitro and in vivo to promote the growth of colorectal cancer cells. e20176 in Heliyon, 9(10).
Zhang LT, Shi SJ, Chu GY, et al. 2023b. By maintaining voltage-dependent anion channel 2, deubiquitinase UCHL1 controls the synthesis of estradiol. Biological Chemistry Journal, 299(11): 105316.
Sirotkin AV (1994). Melatonin's direct effect on cyclic nucleotide release by granulosa cells isolated from pig ovaries, as well as steroid and Nona peptide hormones. Pineal Research Journal, 17(3): 112–117.
Stouffer RL, Xu J, and Ting AY. 2015. distinct effects of progesterone and estrogen on the in vitro formation of secondary follicles in primates in a steroid-depleted environment. 1907–1917 in Human Reproduction, 30(8).
Hsu CC, Vann KR, Sharma R, et al. 2025. Histone H3K36 and H3K4 methylation and ASH1L's structure-function connection. 16(1): 2235 in Nature Communications.
Zhao XY, Wei YH, Shen XX, et al. 2024. By disrupting the miR-218-5p/INHBB axis, circular RNA circRPS19 stimulates the growth of chicken granulosa cells and the production of steroid hormones. 103–115 in Theriogenology, 219.
Peng Y, Xie WQ, Xi H, et al. 2020. In a Chinese family, intellectual disability is linked to a microdeletion on chromosome 1q22, which includes ASH1L.